POLISH MARITIME RESEARCH 4 (128) 2025 Vol. 32; pp. 107-118
10.2478/pomr-2025-0054

NDT-Based Determination of Key Performance Elements of a Ship Propeller Model Manufactured with the Selected Laser Melting Method

Alperen Doğru [1]
Ayberk Sözen [2]
Erkin Altunsaray [2]
Akile Neşe Halilbeşe [3]
Haşim Fırat Karasu [4]
Serkan Türkmen [5]
Gokdeniz Neser [2,*]
[1] Ege University Aviation Higher Vocational School, İzmir, Turkey
[2] Dokuz Eylul University Institute of Marine Sciences and Technology, İzmir, Turkey
[3] Newcastle University School of Engineering, Marine, Offshore & Subsea Technology Group, Newcastle Upon Tyne, United Kingdom
[4] Dokuz Eylul University Engineering Faculty, Mechanical Engineering Department, Izmir, Turkey
[5] Tallinn University of Technology, Estonian Maritime Academy, Tallinn, Estonia

* Corresponding author: *gokdeniz.neser@deu.edu.tr (Gokdeniz Neser)*

ABSTRACT

Additive Manufacturing aided by 3D printers (3DAM) is seen as an alternative to conventional manufacturing (CM) methods, especially in terms of sustainability, mitigating the inefficiencies and constraints of CM methods. Metal-based 3DAM is highly variable, in terms of speed, accuracy, material compatibility, and application-specific suitability. In this study, a ship propeller model, made of AlSi10Mg powder alloy using Selective Laser Melting (SLM (which is a widely used 3DAM method), was examined for both surface and internal deficiencies through non-destructive testing (NDT) methods after operating the model under cavitation tunnel conditions for a specific period. It was observed that the factors that determine the production quality of the propeller model are: (1) consistency of the dimensions of the resulting product with the original design; (2) surface roughness and the quality of the treatment(s) to be applied to eliminate it; (3) voids forming in the internal structure; and (4) ageing of the propeller in the marine environment.

Keywords: additive manufacturing of ship propeller, selective laser melting (SLM), AlSi10Mg Alloy, non-destructive testing (NDT), key performance elements of an additively manufactured metal propeller

INTRODUCTION

Additive manufacturing using 3D printers (3DAM) offers the advantage of producing complex geometries without extensive post-processing but with minimum material waste, competitive costs and low production volumes [1]. These capabilities benefit the production of customised products and special parts, such as ship propellers and rotor blades with complex geometries [2]. 3DAM has also brought an innovative approach to the cutting-edge technologies and tools which are used to manufacture complex parts through other methods [3].

Among the 3DAM methods, Selective Laser Melting (SLM) selectively fuses powdered materials layer-by-layer with a high-powered laser and is effectively used to produce metal parts with high precision and complex geometries [4]. SLM is crucial for Research and Development (R&D) applications in the aerospace, automotive, and maritime industries [5]. For example, the argument that SLM would be rapid and cost-effective in producing high-quality propellers has begun to appear in the literature [6].

The use of AlSi10Mg, which is considered to be lightweight and of high-strength in the SLM method, is becoming increasingly popular. In addition, this corrosion-resistant material can be seen as an opportunity for developing the sustainable production of structural marine elements [7,8]. With such lightweight structures, less fuel consumption, less materials, lower labour costs, and lower maintenance-repair costs can be guaranteed [8,9]. Approval of these products is currently being considered by the classification societies [10].

However, problems such as porosity and roughness on the surfaces of metallic products produced with 3DAM methods can cause weak or broken interlayer bonds and micro-cracks are frequently encountered in their internal structures. These negatives, particularly when marine conditions are considered, also shorten the product life by casting doubt on the safety of the operation of vehicles under various environmental loads. In order to prevent this damage, precautions should be taken during the design phase of the structure (e.g. rounded edges against stress accumulation, optimised layered structure, etc.), as well as post-processing (e.g. surface coating and hardening, heat treatment, etc.). As the most common surface treatment method, epoxy or polyurethane coating is used because it is resistant to environmental effects. Special paints can be produced for the relevant metal and anodising, which forms a thick protective oxide layer on the surface, is also used [11]. In addition, ceramic coating is an option because it is stiff, highly resistant to environmental effects, and has a wear-resistant surface [12].

In recent years, studies have been conducted using non-destructive testing (NDT) methods, such as X-ray tomography, thermographic examination, and optical microscope imaging [13] to improve the fatigue strength of 3DAM products made of AlSi10Mg alloy. Qian et al. [14] examined the development of fractures in AlSi10Mg products produced with the SLM method by using X-ray tomography and determined the critical role of defect morphology on performance. With the same NDT method, Wang et al. [15] investigated the adverse effects of holes in the material on shear strength, both experimentally and numerically, by modelling with the Finite Element Method (FEM). Romana et al. [13] compared the effectiveness of this manufacturing method with an optical microscope. They found it to be superior and more cost-effective for analysing large volumes of materials. Similarly, Pascual et al. [16] measured the effects of the size, shape, and location of the voids in the material on its mechanical performance through X-ray tomography. Ngnekou et al. [17] also determined that the T6 heat treatment of products produced with the same material and method improved the microstructure in a way that would increase fatigue performance and cause silicon precipitates. In addition, Tradowsky et al. [18] showed that the recycled powder additive would reduce the tensile performance of the alloy. Jian et al. [19] thought that the powder sizes also affected the high-cycle fatigue behaviour and experimentally showed that large sizes (min. 50 μm) provide better fatigue performance than small sizes (smaller than 20 μm) because crack initiation starts more easily around small-sized particles which have not melted.

In contrast, larger-sized particles can lead to sub-surface crack initiation. Chen et al. [20] examined the effect of part size on fatigue performance. They showed that large-sized parts have lower performance and that areas where fusion is not fully developed and gas pores are present are prone to crack initiation.

Propellers are one of the most complex components of ships and have become the focus of much research in recent years, due to their designs, new manufacturing methods and materials, and the damage they may encounter during their operational life. Recent research has addressed several aspects of propeller design and diagnostics. Samsul [21] examined how adding a blade cup reduces cavitation and compared cupped and non-cupped propellers' thrust, torque, and efficiency. Kluczyk et al. [22] reviewed diagnostic methods for polymeric propellers, noting that composite materials offer weight reduction and hydro-elastic advantages but require tailored non-invasive inspection techniques. Zheng et al. [23] developed a reverse-engineering-inspired parametric 3D geometry model for marine propellers and demonstrated that the reconstructed models accurately reproduce hydrodynamic performance. Zinati et al. [24] used computational fluid dynamics to quantify how fouling roughness degrades thrust and efficiency. Grządziela et al. [25] validated a lifting-surface-based FEM model incorporating hydro-elasticity for propeller design. These studies underline the importance of cavitation control, diagnostic methods, accurate geometric modelling, surface condition, and the structural modelling of propellers.

Despite being documented in related studies, FEM-based models were not included in this work. The focus of this study is restricted to ageing analysis and experimental non-destructive evaluation.

In this study, a ship propeller model, produced from AlSi10Mg alloy using the SLM method, was studied to determine the factors affecting the performance of the material. For this purpose, the geometrical compatibility of the propeller produced with the original design was measured using sensitive 3D scanning and the surface roughness was measured using appropriate equipment. Three different coatings (alodine, anodised, and solvent-based paint) were applied to eliminate surface roughness and the effectiveness of each was analysed under accelerated ageing. After the propeller was exposed to 106 cycles in the cavitation tunnel, the internal damage was determined using X-ray radiography and micro-CT; surface damage was determined using a penetrant test. In addition, a FEM-based propeller model was created and validated using the experimental results. The findings were transformed into suggestions for ways in which marine construction component makers and designers should use this 3DAM technique and alloy.

MATERIALS AND METHODS

PROPELLER MODEL GEOMETRY

In this study, the form properties of a five-bladed propeller made from aluminium alloy material using the SLM method are given in Table 1; its form is presented in Fig. 1. The blade loading distribution was adapted through wake-induced adjustments. In contrast, the thickness distribution was modified beyond 0.8R towards the blade tip for optimised performance. Instead of a standard benchmark propeller, a fixed-pitch propeller (designed for the EU 'Gaters' project) was used [5].

Table 1. Propeller geometry

Property Description	Value
Propeller diameter (D),	0.2571 m
Pitch to diameter ratio (P/D) at 0.7R	0.83
Expanded Area Ratio (EAR)	0.466
Number of blades	5
Rake angle	0°
Skew angle (back)	14.62°
Direction of rotation	Right-handed turning
Hub diameter to propeller diameter ratio	0.18
Blade thickness at 0.75R	0.003 m

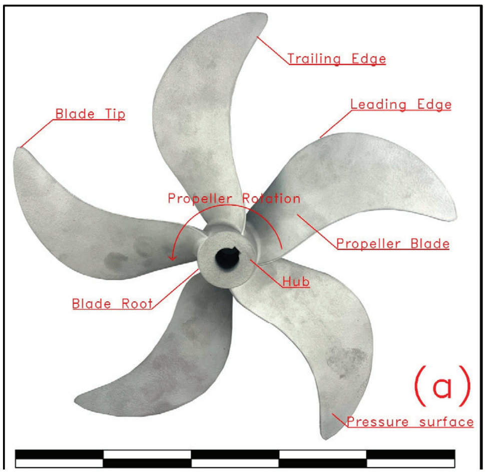

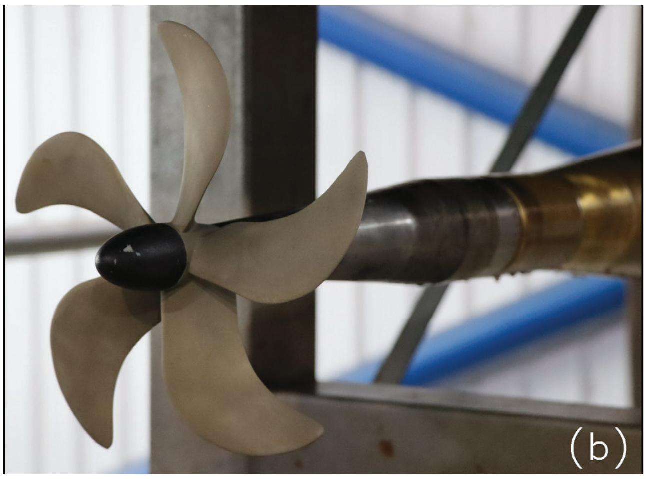

Fig. 1. (a) Propeller geometry and (b) cavitation tunnel test setup

MATERIAL AND 3DAM

The final properties of the materials manufactured using the SLM method using AlSi10Mg powder alloy are presented in Table 2.

Table 2. AlSi10Mg properties [26]

Property Description	Value
Density (g.cm^{-3})	2.61
Longitudinal Young's Modulus (E11), MPa	76600
Transversal Young's Modulus (E22), MPa	76600
Longitudinal Shear Modulus (G12), MPa	28790
Longitudinal Poisson's ratio (v12)	0.33
Ultimate longitudinal tensile strength, MPa	395
Ultimate longitudinal compressive strength, MPa	480
Ultimate transverse tensile strength, MPa	395
Ultimate transverse compressive strength, MPa	480
Ultimate in-plane shear strength (S12), MPa	223

The propeller was manufactured using Kings Company's M280 model printer (Republic of China). After production, the propeller was sintered, followed by a sandblasted surface treatment. Additionally, the sample plates (measuring 50 × 50 mm, with a thickness of 3 mm) were used for surface treatment tests.

The printing direction during the additive manufacturing process was 0°, as seen in Fig. 2, which meant that the propeller was printed vertically, with the blade surfaces parallel to the build platform. This orientation is commonly used to reduce support material at the leading and trailing edges and to minimise stair-step effects on the blade surface. However, vertical build orientation can also increase susceptibility to anisotropic mechanical behaviour and defect alignment along the build axis, which may influence fatigue crack initiation.

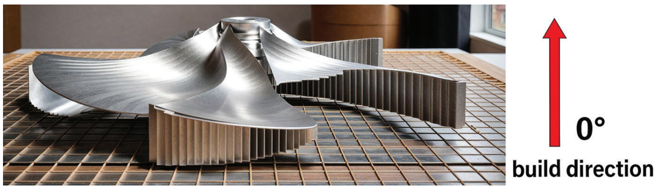

Fig. 2. Printing directions of the propeller

In order to ensure the structural reliability and hydrodynamic efficiency of the propeller, a dimensional verification study was performed following the printing process, to assess the geometric conformity of the manufactured component with the original CAD model. This verification study was performed to identify potential deformations, thermal-induced distortions, or build-related deviations that may adversely affect the propeller's performance under operational conditions.

For this purpose, the as-printed propeller was scanned using a handheld Hexagon Atlas Scan laser scanner (Hexagon

AB, Sweden, 2023 model). Data acquisition was carried out using HHSCAN v2.1.4 (Beijing HiHope, China) and the resulting 3D point cloud was processed and analysed using PolyWorks Inspector™ 2023 IR4 (InnovMetric Software Inc., Canada), which is a widely used metrology software for quality inspection and CAD comparison in manufacturing.

Using a best-fit alignment algorithm, the scanned geometry was aligned with the reference model. A colour-coded deviation map was generated to visually and numerically assess dimensional deviations. Thirty-one control points, distributed across the blade and hub surfaces, were selected for quantitative evaluation. Tolerance values were set at ±0.500 mm, as per the ISO 1101 [27] standard, and typical additive manufacturing tolerances were assumed for functional metallic parts.

PROPELLER MATERIALS, COATINGS, AND AGEING

Three different coatings were applied to prevent wear on the propeller during cavitation tunnel testing: chromate (alodine) coating (alodine/200/1200s), an anodised layer formation, and synthetic solvent-based painting. A sample without any coating was also produced, for control purposes.

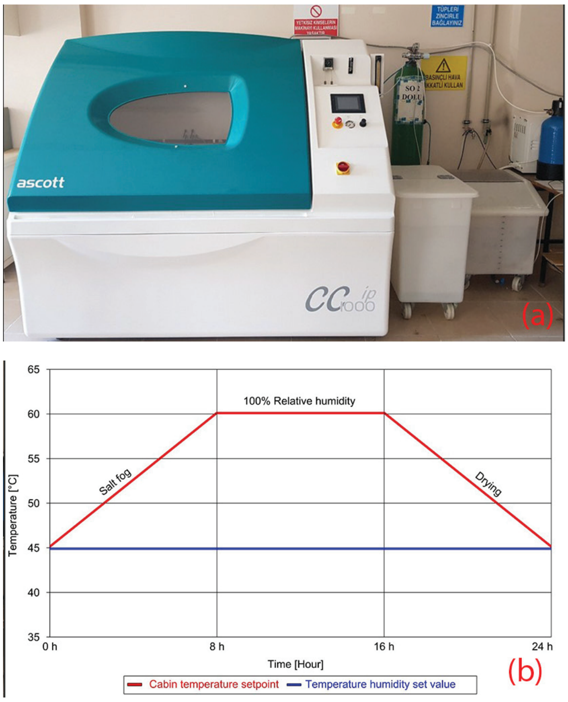

Fig. 3. (a) Ageing chamber, (b) Ageing cycle

Alodine coating is a chemical process that forms a protective layer of film on aluminium alloys to enhance their corrosion resistance. The coating process for the samples was performed according to the MIL-C-5541 standard [28], using the Class A type method. Unlike traditional coatings, anodising does not involve applying an external layer; instead, it oxidises the aluminium surface, forming a hard protective layer through anodic film formation. During the anodising process, the sample was subjected to an electrochemical reaction in an acidic solution, where the sample acted as the anode and the solution served as the electrolyte. For the synthetic painting process, a solvent-based paint with superior adhesion properties was used. The samples were coated with Müller-brand light grey synthetic solvent-based paint. To examine the effects of wear on all samples, including the uncoated control group, an ageing process was conducted in an ageing chamber.

Accelerated ageing tests were performed in accordance with the ASTM B117 [29] and ISO 9227 [30] standards in the CC1000ip model test chamber at Ascott Company (United Kingdom), with the apparatus shown in Fig. 3. The reason for choosing this type of accelerated ageing test device was to provide the samples (dimensions 12.5 x 12.5 x 0.5 mm) with cyclic ageing conditions which were the closest to atmospheric conditions. The chamber had a cabin volume of 1000 l and a saltwater compartment volume of 115 l; it operated at 4-6 bar air pressure, with a salt spray capacity of 0.5-3.0 ml.h-1 over 80 cm2. The samples were placed in the ageing test chamber so that all surfaces were affected by moisture and salt. The saltwater solution in the test chamber contained 3.5% NaCl, to simulate sea conditions. Samples were exposed to saltwater in the chamber at an inclination of 150-300°. As seen in Fig. 3, the 24-hour ageing cycle was divided into three equal time periods, in accordance with the relevant standards [28–30] the first eight hours comprised testing with water vapour at 60 °C, the second eight hours with salt water vapour at 45 °C, and the last eight hours with drying at 60 °C. Ageing was applied for a total of 21 days.

NDT METHODS APPLIED

Optical microscopy

After the ageing process, the surfaces of both the surface-treated samples and the control group samples were examined under an optical microscope. The images were obtained using a Zeiss Primostar 3 (Germany) optical microscope at 40× magnification and a diameter of approximately 0.5 mm.

Before microscopy, the samples were cleaned with ethanol and gently dried with compressed air to remove residual salts and moisture. No additional surface polishing or etching was applied, to preserve the actual ageing-induced features. The analysis focused on surface wear, salt accumulation and intake, and the initiation of deformations, especially at vulnerable edges.

Micro-CT test

As a 3DAM, SLM can cause internal defects such as porosity, which may affect the mechanical properties of the final component. To assess the volumetric density and porosity levels of the manufactured aluminium samples, Micro-Computed Tomography (Micro-CT) analysis was performed. This non-destructive technique allows for a detailed evaluation of internal structures, facilitating the identification and quantification of voids within the material.

The volumetric density and voids in the specimens were also determined using Micro-CT imaging, to assess the manufacturing performance. The Micro-CT tests were conducted using the μCT50 model device from SCANCO (Switzerland) at the Ege University Central Research Test and Analysis Laboratory Application and Research Centre. A 3 mm^3 section of each specimen was scanned at 90 kVp energy, 155 μA intensity, an integration time of 300 ms, and a voxel size of 5 μm, to obtain high-resolution imaging of its internal structure.

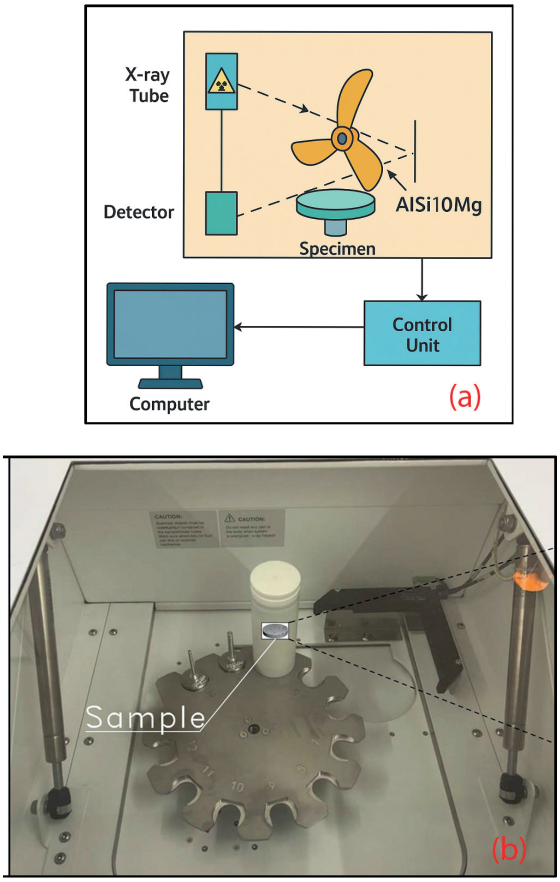

Fig. 4. (a) Micro-CT System Diagram, (b) Samples in the chamber

In micro-CT, the porosity percentage of a sample is critical and is used to assess the internal structure. This parameter quantifies the proportion of void spaces (pores) within the total volume of the scanned object. The system diagram of the micro-CT setup used for such analyses is presented in Fig. 4.

X-ray imaging

The internal structural inspection of the manufactured propeller was performed using radiographic inspection, which employs high-energy X-rays to penetrate the propeller and generate detailed images of its internal structure using a LORAD LPX160 device (USA), as seen in Fig. 5. Based on the average thickness values of these critical regions, the aluminium propeller was exposed to 80 kV energy and 2.5 mA for a duration of 5 minutes, to ensure optimal imaging and defect detection.

Fig. 5. (a) X-ray device, (b) control panel, (c) X-ray film of the propeller

Penetrant tests

The penetrant inspection method, commonly used for detecting surface discontinuities, was applied to evaluate manufacturing-induced defects and potential defects formed after the performance test. The test procedure was conducted in accordance with the ASTM E1209 [31] standards. Following Method A, a type I fluorescent penetrant was applied to the propeller's surface. The penetrant inspection was conducted after manufacturing and, also, following the performance test, to ensure the detection of any potential surface discontinuities in the propeller (Fig. 6).

Fig. 6. Application steps of penetrant on the propeller surface: (a) The propeller was positioned for penetrant application,(b) The immersion technique was used to ensure complete surface contact with the penetrant,(c) The penetrant was evenly spread over the surface,(d) Excess penetrant was removed using a 40 PSI pressure water spray gun at room temperature,(e) The propeller was dried at 60 °C for 20 minutes,(f) A developer was applied to make any discontinuities visible,(g) Dwell time was observed,(h) The test was performed in a darkroom under UV light to detect potential defects

Cavitational tunnel tests

The propeller was tested for 50 hours at 900 RPM, which corresponds to approximately 10^6 cycles. Open-water experiments were performed at Newcastle University's Emerson Cavitation Tunnel to assess the propeller's efficiency and cavitation characteristics under controlled conditions (Fig. 8). As shown in Fig. 7, the propeller model was mounted on the tunnel's Kempf & Remmers H45 dynamometer (Germany), allowing for precise measurement of the thrust, torque, and efficiency [5,32]. The standard ITTC procedure for data acquisition was followed [33].

The experiments were performed under atmospheric conditions at a range of advanced speed coefficients (J) from 0.3 to 0.9, as calculated using Eq. (1).

$$J = \frac{V}{nD} \quad (1)$$

where V is the tunnel water velocity (m·s^{-1}), and n is the shaft rate of the propeller (rps).

The propeller rotation speed was 16 rps and the tunnel velocity was adjusted from 1.23 to 4.10 m.s^{-1} in order to operate the propeller under different loading conditions. The cavitation number was calculated based on the rotational speed defined in Eq. (2).

$$\sigma_n = \frac{P_a + \rho g h_s - P_v}{0.5_{\rho}(nD)^2} \quad (2)$$

where ρ is the water density, h_s is propeller shaft immersion depth, P_a is atmospheric pressure, while P_v is vapour pressure of the water. The cavitation number was calculated as 12.3, which is high. In fact, no cavitation was observed. Further details of the propeller were presented in the study carried out by Altunsaray et al. [5] including the hydrodynamic and cavitation performances.

Fig.7. Cavitation tunnel test

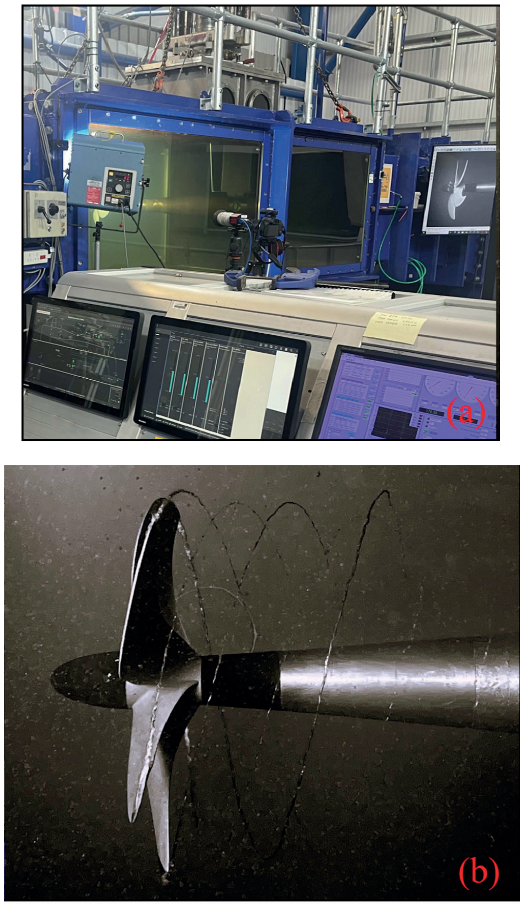

Surface roughness measurement

After the tunnel and cavitation testing (conducted in a cavitation tunnel), surface roughness measurements were conducted to evaluate their effect on the propeller's performance, as seen in Fig. 9. The measurements were performed using a Taylor Hobson Surtronic 3+ Surface Profilometer, following the ISO 2009 [34] standard for surface roughness assessment. The analysis focused on key parameters, including the arithmetic mean deviation (Ra) and total height (Rt), to quantify surface texture variations and identify potential impacts on hydrodynamic efficiency and fatigue resistance.

Fig. 8. Surface roughness measurement

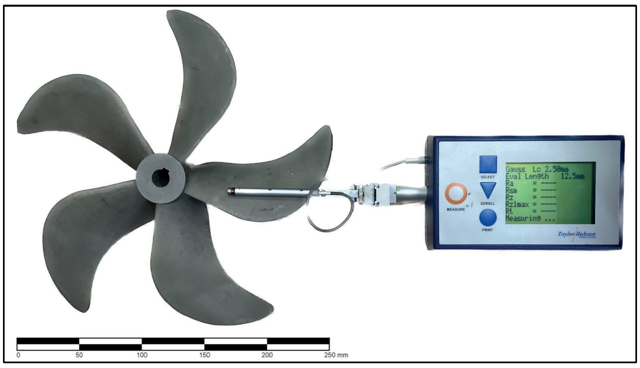

RESULTS AND DISCUSSION

GEOMETRY CHECK

Fig. 9 shows the colour codes for deviations obtained with PolyWorks. There are significant deviations between the dimensions of the propeller as the final product and the nominal dimensions of the design of the propeller, resulting from manufacturing after the precise 3D scanning process.

The deviations are generally within an acceptable tolerance range of ± 0.500 mm [27]. It was determined that, due to the propeller having five blades and lacking a symmetrical geometry, the geometric tolerance was compromised in areas where the thickness was below 2 mm, and each blade exhibited different geometric tolerances. The areas exceeding this tolerance are in relatively thin sections near the tips and edges of the propeller blades, e.g. surf pt 4 (-0.502), pt 20 (-0.518), and pt 31 (+0.520).

Of course, these deviations would be expected to negatively affect the propeller's hydromechanical performance due to the microvortices they create throughout the propeller area. The results underscore the need for geometrical refinement in critical blade regions, especially near the trailing edge and blade root, where stress concentrations and flow separation are most sensitive to form deviation. Selective post-processing may be necessary to mitigate the impact of dimensional inaccuracies in future manufacturing.

Also, changes can raise the electrical differences on the propeller surface, making it easier for corrosion to start and spread. Considering these deviations, the improvement of the propeller form in the design phase can be achieved by developing a design-for-zero-deviation approach.

The detection of deviations after production in 3DAM is essential for improving subsequent production, both in the design phase and in determining the post-processing to be selected. In other words, the understanding that 3D scanning of the final product should be an integral part of production should be established.

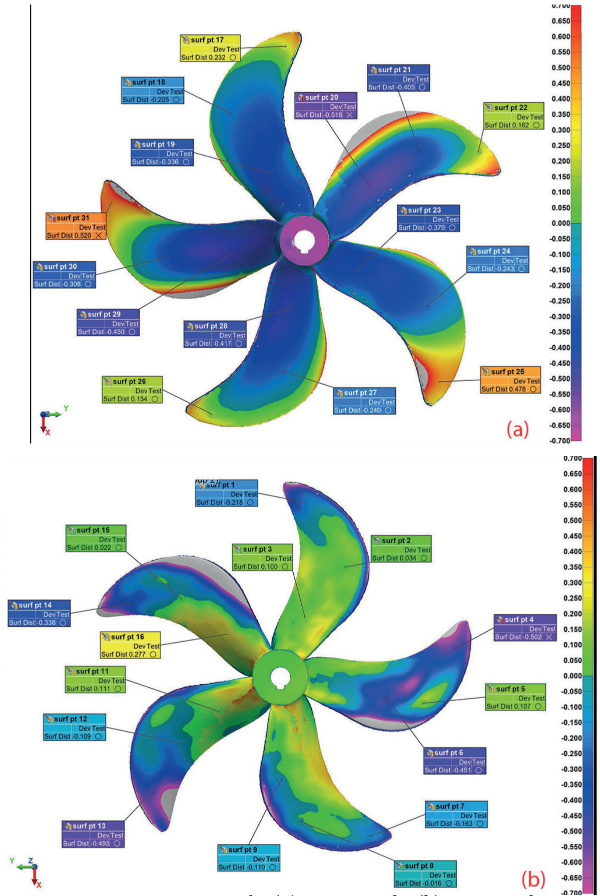

Fig. 9. Deviations on the (a) pressure side, (b) suction side

AGEING PERFORMANCE

After applying three different surface treatments, accelerated ageing tests were conducted to assess the propeller's resistance to environmental ageing effects. Following these tests, the surface morphology of the samples was examined using an optical microscope. The results are presented with the ageing times in Fig. 10.

In the uncoated control group (AlSi10Mg), surface degradation, in the form of wear and significant colour change, was observed, indicating corrosive activity. The mass measurements taken before and after the ageing process confirmed material loss due to wear, further highlighting the importance of surface protection.

Alodine 1200 / 1200S, a hexavalent chromate conversion coating, was used in this study due to its widespread application in the aerospace industry. Known for its distinctive metallic gold coating finish, this coating forms a durable protective layer that significantly enhances corrosion resistance. It is particularly preferred for use with aluminium alloys in aircraft structures, where long-term durability and surface integrity are critical. Although slight abrasion was observed on the coating after the accelerated ageing process, the underlying material remained unaffected. This indicates that Alodine 1200S effectively prevents deep penetration of corrosive agents and maintains surface protection under harsh environmental conditions.

The spray-painted sample, coated with an acrylic-based paint, formed a protective layer. However, after ageing, small pits and signs of local corrosion appeared. These pits, and the change in colour, indicated that the corrosion had passed through the paint and reached the metal surface, which reduced the paint's protective effect.

In contrast, the Type II anodised sample developed a surface oxide layer, providing a moderate corrosion protection level. However, this layer also resulted in measurable material loss due to surface oxidation. Additionally, the surface showed the adhesion of environmental particles, such as salt crystals, dust, and airborne contaminants, which became trapped within the porous anodised layer. This led to a noticeable increase in the overall weight of the sample after ageing (Table 3). Its porous structure makes it easier for small particles to get stuck on the surface, especially after prolonged exposure to marine-like environments.

Alodine coating seems to be the best solution for the propeller made from aluminium alloy via the SLM method in this study, due to the low ageing effects and the lightness of the coating throughout the process.

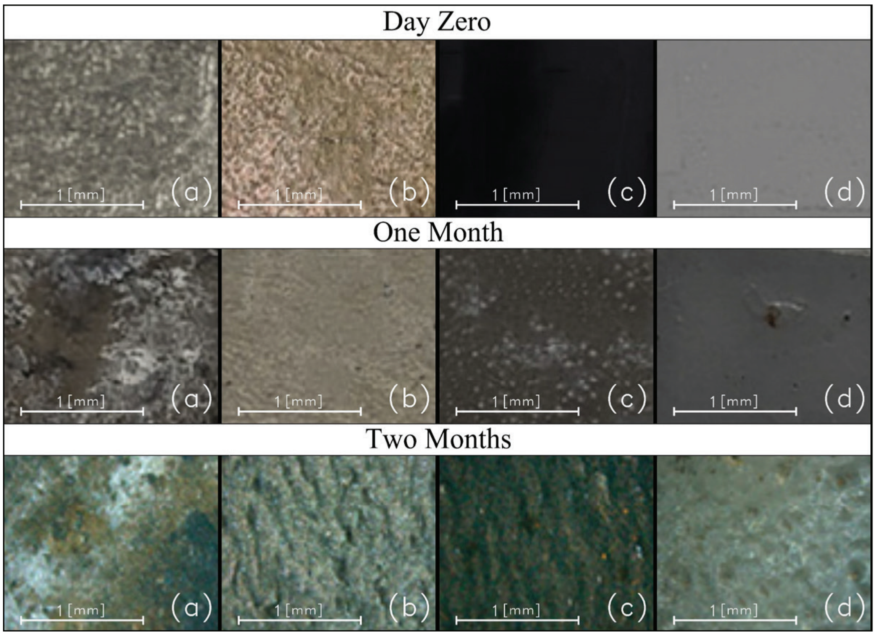

Fig. 10. Performance of surface coatings in the climate chamber: (a) Uncoated / control, (b) Alodine coated, (c) Anodised, and (d) Paint coated

Table 3. Sample weights (g)

Conditions	[a] (Uncoated)	[b] (Alodine)	[c] (Anodised)	[d] (Painted)
Before coating	0.215	1.290	1.265	0.619
After coating	0.215 (0%)	1.293 (+0.23%)	1.264 (-0.08%)	0.641 (+3.43%)
After ageing of the coated sample	0.211 (-1.9%)	1.291 (-0.15%)	1.266 (0.16%)	0.64 (-0.16%)

(1) *Values in parentheses indicate the percentage of weight change.*

MICRO-CT TEST

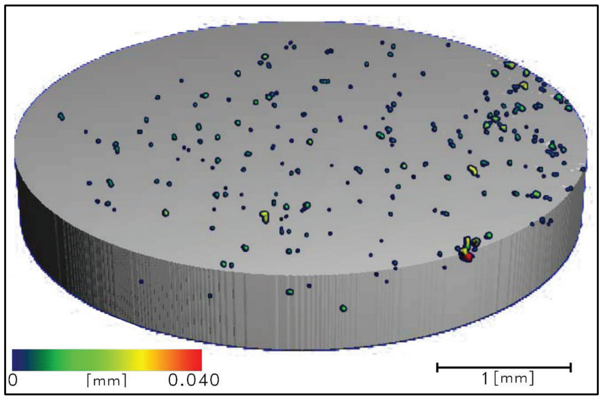

Fig. 11 Porosity

Based on micro-CT reconstruction, Fig. 11 shows a colour-coded map of the sample's void distribution; the uniformly distributed porosity of 0.04% suggests efficient melting and a lack of significant pore clusters.

The results indicate a low porosity level, which aligns with expectations for the SLM-produced aluminium components. Similar studies in the literature report porosity percentages in the range 0.01- 0.10%, depending on process parameters such as laser power, scanning speed, and powder layer thickness [35].

Micro-CT imaging further confirmed that the porosity was uniformly distributed within the sample, with no significant clustering of voids. This uniformity is crucial for ensuring consistent material properties throughout the component. Research has highlighted that excessive porosity can lead to reduced mechanical strength, increased fatigue susceptibility, and compromised thermal conductivity. Therefore, maintaining porosity within the expected range is essential for the reliability and durability of SLM-fabricated parts. This study demonstrates the effectiveness of the selected manufacturing parameters in producing high-density components with minimal internal defects. Future studies could further refine the process by adjusting energy input, hatch spacing, and powder bed conditions, to achieve even lower porosity levels, thereby enhancing the mechanical properties of SLM-produced aluminium components.

X-RAY TESTS

No process-related discontinuities were observed in the propellers manufactured using the Selective Laser Melting (SLM) method. The X-ray test performed after pre and post-cavitation tunnel testing confirmed the structural integrity of the propeller and the corresponding radiographic image is presented in Fig. 12.

Fig.12 shows that the cracks were detected in the root of the blades after the performance test. This meets the expectation that the stress concentration will occur at the propeller root, where the most significant moment arises during operations.

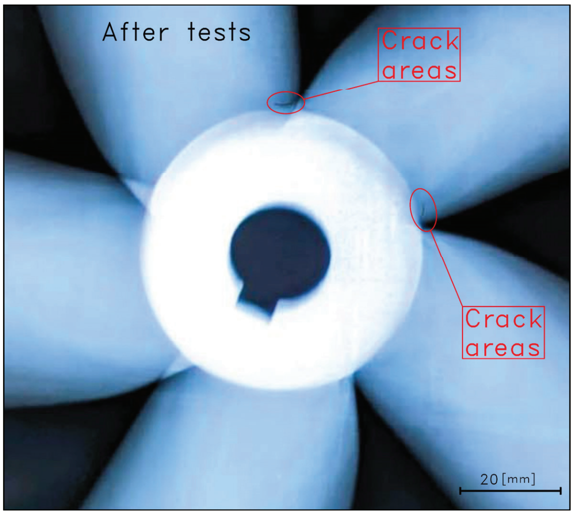

Fig. 12. Cracks detected on the X-ray film

Moreover, these findings provide additional data regarding the performance limits of SLM-manufactured propellers. The observed fatigue cracks and their initiation points help clarify potential durability issues in additively manufactured marine components, highlighting the importance of further optimisation in structural design and manufacturing parameters.

PENETRANT TESTS

The manufactured propeller was also subjected to penetrant testing to inspect for surface discontinuities. As seen in Fig. 13(a), the penetrant inspection confirmed the findings of the post-production X-ray test; there was no evidence of surface imperfections caused by the production. This verification further supports the integrity of the SLM manufacturing process in producing defect-free components at the surface level.

However, after the cavitation tunnel tests, X-ray imaging detected cracks at the root sections of two blades. The penetrant inspection confirmed that these cracks were surface defects (Fig. 13(b)).

The penetrant test results demonstrated that SLM-manufactured propellers do not exhibit post-production surface discontinuities. However, operational loads can lead to crack formation in high-stress regions, particularly at the blade roots. Identifying surface-breaking cracks highlights the importance of defect-resistant design strategies and post-processing treatments to enhance the durability of additively manufactured propellers. The lack of fusion pores and unmelted particles act as micronotches, markedly reducing endurance strength; crack nuclei are frequently traced to such defects in SLM AlSi10Mg [36].

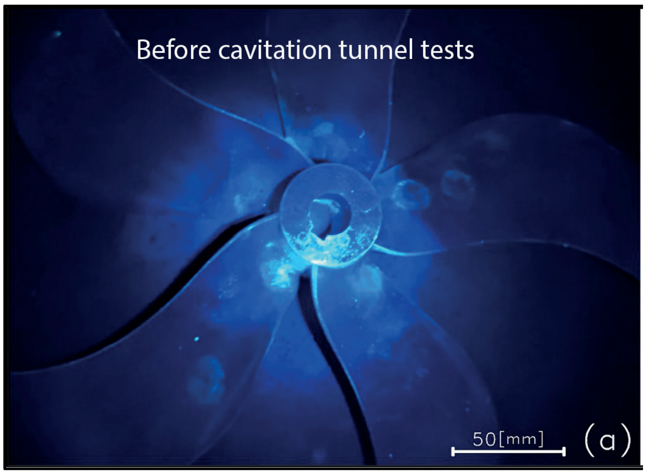

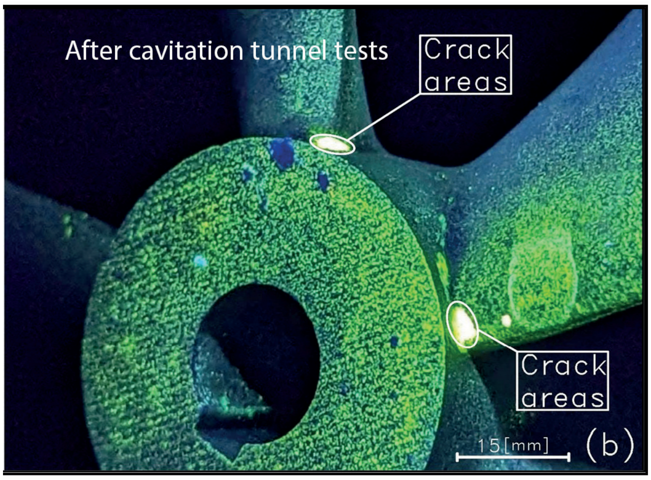

Fig. 13. Cracks detected in the penetrant test (a) before the test, (b) after the test

SURFACE ROUGHNESS

When the surface roughness of the propeller is considered, based on the ITTC [34] approach on this issue (which states that the total roughness should not exceed 25 µm and the arithmetic mean roughness should not exceed 5 µm), it can be seen that the values of the propeller produced in this study are reasonably high (see Fig. 14). It is strongly advised to apply polishing, sandblasting, and chemical methods to propellers produced with SLM.

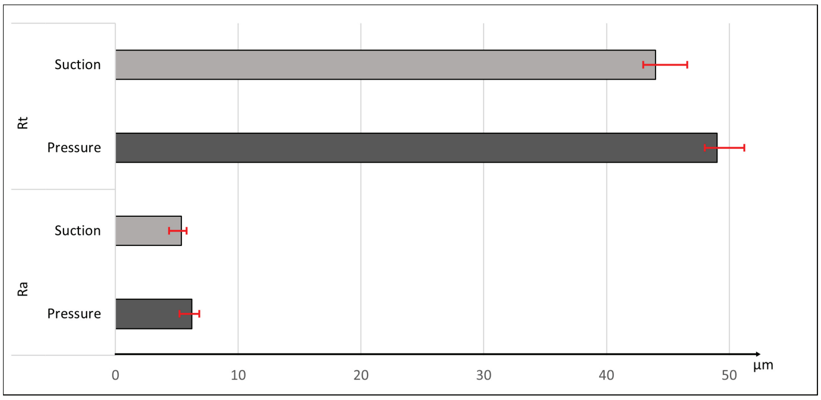

Fig. 14 Surface roughness measurement results, Ra and the total height Rt describe the average roughness and the total height of the roughness

(energy, temperature, speed, etc). This is a current problem that can be answered with further experimental studies.

4. **The ageing of a propeller in a marine environment** is a serious factor that should be taken into consideration from the design stage onwards. One of the coating methods suggested by different researchers (including this study) should definitely be applied to the products.
5. It is evident that special experimental studies are necessary, in order to determine the root causes of defects that occur during the production (lack of fusion pores, unmelted particles, etc.) and operation of the propellers (pressure shocks, thermal effects, vibrations, etc).

CONCLUSIONS

This study investigated the factors affecting the performance of a propeller model produced with AlSi10Mg material using the SLM (one of the 3DAM methods) and NDT methods. These tests were carried out after cavitation tunnel testing of the propeller, to examine the results of a particular loading condition and the effects of three different coatings, depending on the ageing processes. In this context, in addition to the tests relating to the quality of the product's surface, optical microscopic observations, roughness measurements, penetrant tests, X-ray radiographic tests, and Micro-CT imaging were carried out to investigate the product's internal structure.

This study demonstrates that the SLM method can produce aluminium propellers with low porosity (0.04%) and acceptable dimensional accuracy after stress relief. However, as-printed roughness values (Ra ≈ 10–20 µm, Rt ≈ 40–80 µm) exceed ITTC recommendations, requiring post-processing. Among the coatings tested, alodine conversion coating provided the best ageing resistance. Cavitation tunnel testing revealed fatigue cracks in the blade roots, highlighting the need for improved build orientation and reinforcement. These findings provide quantitative guidance for using the SLM method of 3DAM in marine propeller manufacturing.

The following issues have come to the forefront as key performance elements for propellers manufactured with the method and materials in this study, considering the NDTs performed:

1. **Geometric consistency of the dimensions of the resulting product, in relation to the original design,** should be measured frequently at critical stages of propeller production and operations. Precise 3D scanning is an indispensable part of this production method.
2. **Surface roughness** is one of the most critical factors affecting propeller performance and should be eliminated as much as possible, through various surface improvement and post-processing methods.
3. **Voids formed in the internal structure** of the propeller should be avoided by adjusting the printing parameters

ACKNOWLEDGEMENTS

The authors would like to thank Hexagon for providing access to their 3D scanning facilities and Abdullah Ata for his valuable support during the propeller scanning process. Dokuz Eylül University funded this study under the Research Universities Support Program (Grant No. FBA-2023-3025).

REFERENCES

1. Wong KV, Hernandez A. A Review of Additive Manufacturing. ISRN Mechanical Engineering 2012; 2012:1–10. https://doi.org/10.5402/2012/208760.

2. itsikoulis SA, Tekumalla S, Sharma A, Wong WLE, Turkmen S, Liu P. Cavitation Hydrodynamic Performance of 3-D Printed Highly Skewed Stainless Steel Tidal Turbine Rotors. Energies (Basel) 2023; 16. https://doi.org/10.3390/en16093675.

3. Horst D, Duvoisin C, Sousa M. Additive Manufacturing at Industry 4.0: a Review. International Journal of Engineering and Technical Research 2018; 8.

4. Hajnys J, Pagac M, Mesicek J, Petru J, Spalek F. Research of 316L Metallic Powder for Use in SLM 3D Printing. Advances in Materials Science 2020; 20: 5–15. https://doi.org/10.2478/adms-2020-0001.

5. Altunsaray E, Turkmen S, Sözen A, Doğru A, Liu P, Halilbeşe AN, Neser G. On the Hydrodynamic and Structural Performance of Thermoplastic Composite Ship Propellers Produced by Additive Manufacturing Method. J Mar Sci Eng 2024; 12: 2206. https://doi.org/10.3390/jmse12122206.

6. Neşer G, Sözen A, Doğru A, Liu P, Altunsaray E, Halilbeşe AN, Türkmen, S.. Improving the Flexibility of Ship Propellers Additively Manufactured from High-Density Polyethylene/Long Carbon Fiber Composites by Prepreg

Coating. Polymers (Basel) 2024; 16. https://doi.org/10.3390/polym16091257.

7. Harsha Vardhan D, Ramesh A, Chandra B, Reddy M. A Review Of Materials Used For Marine Propellers. Mater Today Proc 2019; 18: 4482–90.

8. Eskandarian M, Liu P. A novel maneuverable propeller for improving the maneuverability and propulsive performance of underwater vehicles. Applied Ocean Research 2019; 85: 53–64. https://doi.org/10.1016/j.apor.2019.01.026.

9. Banhart J, Seeliger HW. Aluminium foam sandwich panels: Manufacture, metallurgy and applications. Adv Eng Mater 2008; 10: 793–802. https://doi.org/10.1002/adem.200800091.

10. Sözen A, Neşer G. A Critical Systematic Scoping Review on the Applications of Additive Manufacturing (AM) in the Marine Industry. Polymers (Basel) 2025; 17. https://doi.org/10.3390/polym17010004.

11. Habazaki H, Shimizu K, Skeldon P, Thompson GE, Wood GC, Zhou X. Effects of alloying elements in aluminium anodising. Transactions of the Institute of Metal Finishing 1997; 75: 18–23. https://doi.org/10.1080/00202967.1997.11871137.

12. Wang YM, Tian H, Shen XE, Wen L, Ouyang JH, Zhou Y, Jia DC, Guo LX, An elevated temperature infrared emissivity ceramic coating formed on 2024 aluminium alloy by microarc oxidation. Ceram Int 2013; 39: 2869–75. https://doi.org/10.1016/j.ceramint.2012.09.060.

13. Romano S, Abel A, Gumpinger J, Brandão AD, Beretta S. Quality control of AlSi10Mg produced by SLM: Metallography versus CT scans for critical defect size assessment. Addit Manuf 2019; 28: 394–405. https://doi.org/10.1016/j.addma.2019.05.017.

14. Qian W, Wu S, Wu Z, Ahmed S, Zhang W, Qian G, Withers PJ. In situ X-ray imageing of fatigue crack growth from multiple defects in additively manufactured AlSi10Mg alloy. Int J Fatigue 2022; 155. https://doi.org/10.1016/j.ijfatigue.2021.106616.

15. Wang P, Zhou H, Zhang L, Chen H, Zhu X, Lei H, Fang D, In situ X-ray micro-computed tomography study of the damage evolution of prefabricated through-holes in SLM-Printed AlSi10Mg alloy under tension. J Alloys Compd 2020; 821. https://doi.org/10.1016/j.jallcom.2019.153576.

16. Pascual A, Ortega N, Plaza S, De Lacalle LNL, Ukar E. Analysis of the influence of L-PBF porosity on the mechanical behaviour of AlSi10Mg by XRCT-based FEM. Journal of Materials Research and Technology 2023; 22: 958–81. https://doi.org/10.1016/j.jmrt.2022.11.172.

17. Alhammadi A, Al-Ketan O, Khan KA, Ali M, Rowshan R, Abu Al-Rub RK. Microstructural characterization and thermomechanical behaviour of additively manufactured AlSi10Mg sheet cellular materials. Materials Science and Engineering: A 2020; 791. https://doi.org/10.1016/j.msea.2020.139714.

18. Tradowsky U, White J, Ward RM, Read N, Reimers W, Attallah MM. Selective laser melting of AlSi10Mg: Influence of post-processing on the microstructural and tensile properties development. Mater Des 2016;105:212–22. https://doi.org/10.1016/j.matdes.2016.05.066.

19. Jian ZM, Qian GA, Paolino DS, Tridello A, Berto F, Hong YS. Crack initiation behaviour and fatigue performance up to very-high-cycle regime of AlSi10Mg fabricated by selective laser melting with two powder sizes. Int J Fatigue 2021; 143. https://doi.org/10.1016/j.ijfatigue.2020.106013.

20. Chen H, Wang X, Ren X. Size effect on fatigue performance of SLM-ed AlSi10Mg alloy: Role of defect size distribution. Int J Fatigue 2024; 182. https://doi.org/10.1016/j.ijfatigue.2024.108163.

21. Burak Samsul M. Blade Cup Method for Cavitation Reduction in Marine Propellers. Polish Maritime Research 2021; 28: 54–62. https://doi.org/10.2478/pomr-2021-0021.

22. Kluczyk M, Grządziela A, Batur T. Design and Operational Diagnostics of Marine Propellers Made of Polymer Materials. Polish Maritime Research 2022; 29: 115–22. https://doi.org/10.2478/pomr-2022-0049.

23. Zheng L, Chen S, Chen X, Ji S. Reverse Engineering-Inspired Parametric 3D Geometry Model of Marine Propeller. Polish Maritime Research 2023; 30: 35–47. https://doi.org/10.2478/pomr-2023-0037.

24. Zinati A, Ketabdari MJ, Zeraatgar H. Effects of Propeller Fouling on the Hydrodynamic Performance of a Marine Propeller. Polish Maritime Research 2023; 30: 61–73. https://doi.org/10.2478/pomr-2023-0059.

25. Grządziela A, Kraskowski M, Król P, Szturomski B, Kiciński R. Experimental Validation of an FEM Model Based on Lifting Theory Applied to Propeller Design Software. Polish Maritime Research 2024; 31: 67–76. https://doi.org/10.2478/pomr-2024-0022.

26. Altunsaray E, Turkmen S, Sözen A, Doğru A, Liu P, Halilbeşe AN, Neser G. On the Hydrodynamic and Structural Performance of Thermoplastic Composite Ship Propellers Produced by Additive Manufacturing Method. J Mar Sci Eng 2024; 12. https://doi.org/10.3390/jmse12122206.

27. International Organization for Standardization (ISO). Geometrical product specifications (GPS)-geometrical

tolerancing-tolerances of form, orientation, location, and run-out 1101. Vol. 1101; 2012.

28. American Society for Testing and Materials International (ASTM). Chemical Conversion Coatings on Aluminium and Aluminium Alloys MIL-C-5541; ASTM, 1990.

29. American Society for Testing and Materials International (ASTM). Standard Practice for Operating Salt Spray (Fog) Apparatus B117. West Conshohocken, PA: ASTM International; 2011. https://doi.org/10.1520/B0117-11.

30. International Organization for Standardization (ISO). Corrosion tests in artificial atmospheres — Salt spray tests 9227; ISO, 2017.

31. American Society for Testing and Materials International (ASTM). E1209 Standard Test Method for Fluorescent Liquid Penetrant Examination Using the Water-Washable Process. USA; ASTM, 2017.

32. Türkmen, S., Wang, L., Raftopoulos, S., Li, C., and Norman, R. (2023). *Analysis of the Hydrodynamic Performance of a Gate Rudder System*. In: *IOP Conference Series: Materials Science and Engineering*, vol. 1288. IOP Publishing, Bristol, UK, 012059. https://doi.org/10.1088/1757-899X/1288/1/012059

33. ITTC-Recommended Procedures and Guidelines Testing and Data Analysis Resistance Test; ITTC, Zurich, Switzerland, 2008.

34. International Organization for Standardization (ISO). 4287 Geometrical product specification (GPS). Surface texture: Profile method. Terms, definitions, and surface texture parameters; ISO, 2009.

35. Shrestha S, Starr T, Chou K. A Study of Keyhole Porosity in Selective Laser Melting: Single-Track Scanning with Micro-CT Analysis. Journal of Manufacturing Science and Engineering, Transactions of the ASME 2019; 141. https://doi.org/10.1115/1.4043622.

36. Domfang Ngnekou JN, Nadot Y, Henaff G, Nicolai J, Kan WH, Cairney JM, Ridosz, L, Fatigue properties of AlSi10Mg produced by Additive Layer Manufacturing. Int J Fatigue 2019; 119: 160–72. https://doi.org/10.1016/j.ijfatigue.2018.09.029.